http://dx.doi.org/10.6113/TKPE.2014.19.2.173

3-레벨 T-형 및 NPC 인버터의 전력 손실 비교 분석

알레미파얌[1], 이동춘†

Comparative Analysis of Power Losses for Three-Level T-Type and NPC PWM Inverters

Payam Alemi[1], and Dong-Choon Lee†

Abstract - In this paper, an analysis of power losses for the three-level T-type and neutral-point clamped (NPC) PWM inverters is presented, in which the conduction and switching losses of semiconductor devices of the inverters are taken into account. In the inverter operation, the conduction loss depends on the modulation index (MI) and power factor (PF), whereas the switching loss depends on the switching frequency. Power losses for the T-type and NPC inverters are analyzed and calculated at the different operating points of MI, PF and the switching frequency, in which the four different models of semiconductor devices are adopted. In the case of lower MI, the NPC-type is more efficient than the T-type, and vice versa. The validity of the power loss analysis has been verified by the simulation results.

Keywords: conduction loss, NPC inverter, power loss, T-type PWM inverter, switching loss

1. Introduction

Multilevel inverters have been widely used for the industrial applications, which is an essential and effective solution for medium voltage and high power applications such as AC electric drives, pumps, fans and tractions [1]-[2]. With the multilevel inverters, a lot of advantages of a reduced voltage deviation, less switching stress on each device of inverter system, reductions in the total harmonic distortion (THD), improved efficiency and in some cases possible fault-tolerant operation can be obtained [2]-[4].

Over the years, several topologies of multilevel inverters have been introduced. The well-known typical topologies are the neutral-point clamped (NPC) (shown in Fig. 1), the flying capacitor (FC) and the cascaded H-bridge (CHB) types [3].

Numerous modification and combinations of these topologies have been presented to satisfy specific application requirements or to improve the operating performance. One modified form is the T-type inverter, which is shown in Fig. 2 [5]. Compared with the three-level NPC topology, the count of the switch in the leg is reduced by a half. Instead, an active bidirectional switch is added to the crossbar.

Recently, the efficiency of the power converter has gained an increasing attention in the low voltage applications such as PV (photovoltaic), PFC (power factor correction) and automotive inverters [5]. The power loss analysis for the T-type and NPC three-level inverters has been presented [6]-[10]. Also, the conduction loss of inverters can be found in [11]-[14]. The switching losses can be calculated using the approximations of I-V switching characteristics of IGBT and diode [12], [15]-[16].

However, a more convenient approach of calculating the switching losses using the switching energy has been presented in [15]. Even though a number of estimation methods for the semiconductor losses have been presented [7]-[16], the evaluation of power losses for the different models of commercial products has

Paper number: TKPE-2014-19-2-10
Print ISSN: 1229-2214 Online ISSN: 2288-6281
† Corresponding author: dclee@yu.ac.kr, Dept. of Electrical Eng., Yeungnam University
Tel: +82-53-810-2582 Fax: +82-53-810-4767
[1] Dept. of Electrical Eng., Yeungnam University
Manuscript received July 16, 2013; accepted Feb. 10, 2014

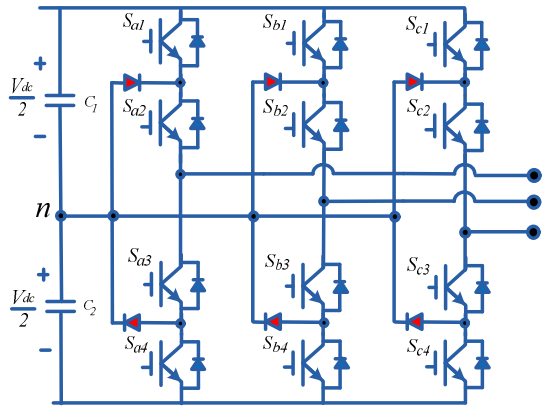

Fig. 1 Three-level NPC inverter

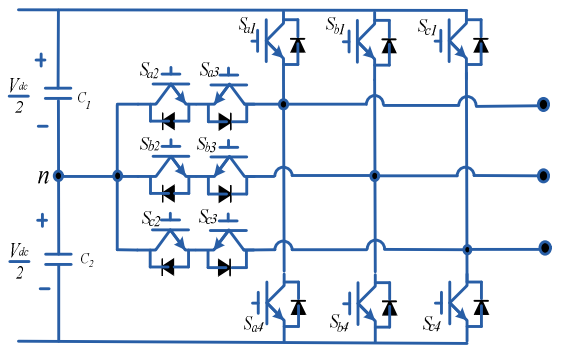

Fig. 2 Three-level T-type inverter

not been carried out.

This paper presents an evaluation of power losses for the three-level T-type and NPC inverters, in which the four different models of semiconductor devices are adopted. The conduction and switching losses for the two types of inverters are analyzed and compared, which shows that in the case of unity modulation index, up to the medium range of switching frequency (8kHz $< f_s <$ 20kHz), the power losses of the T-type inverter is lower than that of the NPC one. On the other hand, with a low MI operation, the power losses of the NPC inverter are lower than those of the T-type even at the low switching frequency. The PF also has an effect on the conduction losses of inverters. In the case of the unity MI and lower PF, the NPC-type is more efficient than the T-type in the medium frequency range.

The analysis results of the power loss are verified by the simulation. In the simulation, the on-resistance and the on/off-switching times are needed to model the conduction and switching loss of IGBTs. The power loss is calculated by the difference of the measured input and output power of inverter.

The results are almost the same with slight errors, which is likely caused by some errors in the simulation conditions and device parameters.

2. Fundamentals of Three-level NPC and T-type Inverters

2.1 Three-level NPC inverters

The three-level NPC inverter is the most widely used topology for medium-voltage industrial applications, which consists of twelve IGBTs and anti-parallel diodes with six clamping diodes. The clamping diodes connected to the neutral point enable to produce a zero voltage level, with which the three different voltage levels are obtained. The NPC three-level inverter has the possibility to use IGBTs and diodes with low breakdown voltages. The lower blocking voltage of devices produces lower losses, from which the efficiency can be increased.

2.2 Three-level T-type inverters

The three-level T-type inverter is a simple extension of the two-level VSC topology with an active bidirectional switch at the DC-link midpoint. The T-type inverter utilizes the advantages of low power losses and simple operation for the two-level inverter and of low THD for the three-level inverter. The main advantage of the T-type topology is the reduced switching losses since the commutation voltage of devices in the leg is only a half compared with that of the two-level inverter [5]. The circuit consists of twelve IGBTs (six 1200-V IGBTs in the leg and six 600-V IGBTs in the crossbar) and twelve anti-parallel diodes. In the T-type inverter, the number of conducted switches in the active current pass is similar to the two-level inverter, which is doubled in the NPC three-level inverter.

3. Calculation of Semiconductor Power Losses

The total power losses of semiconductor devices in the inverters mainly comprise two parts: conduction loss and switching loss. The device leakage loss is not considered since the leakage current during the off-state of the device is negligible.

3.1 Conduction losses

The conduction losses are produced while the power

device is conducting the current in the on-state. Therefore, the power loss during conduction is computed by multiplying the saturation voltage and the current. The saturation voltage is a function of the current, threshold voltage and equivalent resistance of the power devices. The formulas for the conduction losses of the IGBTs in the leg, the bidirectional switches in the crossbar and the anti-paralleled and clamping diodes have been presented in [7], [8]. The conduction losses depend on the MI and PF. The total conduction losses can be calculated by the sum of all IGBTs and diodes conduction losses in the inverter. The conduction power loss of the devices, P_{on} , is computed by multiplying the saturation voltage by the conducting current during the on-time duration, which is expressed as [7]

$$P_{on} = v_{on}|i_c| \tag{1}$$

$$v_{on} = V_0 + R_{on}|i_c|$$

$$i_c = I_c \cos(\omega t - \varphi)$$

where,

v_{on} : saturation voltage,

V_0 : threshold voltage,

R_{on} : on resistance of device,

φ : PF angle,

I_c : peak value of conducting current.

The equations for the IGBT and diode conduction losses in three-level NPC and T-type converters are described in Appendix.

3.2 Switching losses

The switching losses are calculated as a function of the switching frequency, where the turn-on and -off times of IGBTs and diodes are involved. In the fast recovery diodes which are anti-paralleled with the IGBTs, the turn-on losses of diodes are less than 1% compared with the turn-off losses, which is neglected [8]-[12].

3.2.1 IGBT turn-on loss

The turn-on switching behavior of the IGBT is characterized by the turn-on delay time, $t_{d(on)}$, the rise time, t_r, and the turn-on energy E_{on}.

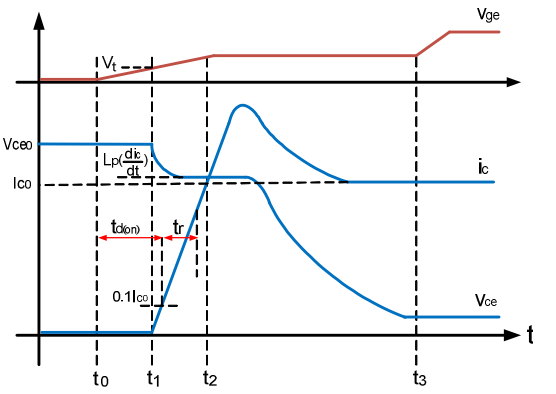

Fig. 3 Switching behavior of IGBT turn-on process

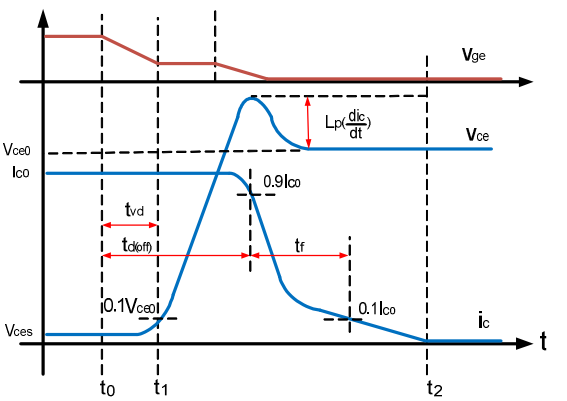

Fig. 4 Switching behavior of IGBT turn-off process

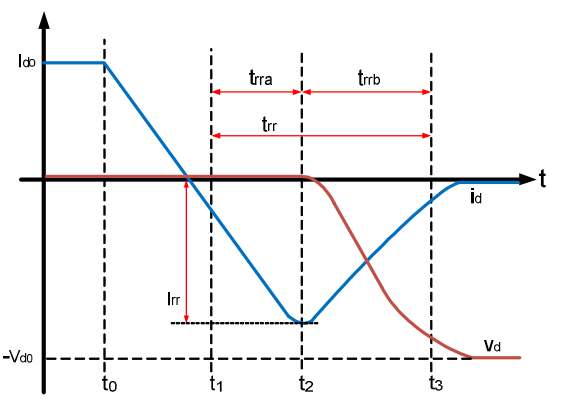

Fig. 5 Switching behavior of diode turn-off process

The turn-on gate pulse is applied at t_0. Due to the input capacitance of the IGBT, the gate voltage, $v_{g.e}$, rises gradually, which is shown in Fig. 3.

After the time $t_{d(on)}$, $v_{g.e}$ reaches the threshold voltage V_t, from which point the collector current i_c begins to increase almost linearly. During the rise

time of i_c, the collector-emitter voltage of the IGBT has a falling part due to the parasitic inductance, which is denoted as L_p. The overshoot of i_c occurs during the time t_2-t_3 due to the reverse recovery current in the free wheeling diodes [5]. The diode reverse recovery current reaches its peak value at t_2, and the collector-emitter voltage, v_{ce}, begins to fall at the same time [9], [12].

3.2.2 IGBT turn-off loss

The IGBT turn-off switching behavior is illustrated in Fig. 4, which is characterized by the turn-off delay time $t_{d(off)}$, falling time t_f, and turn-off energy E_{off}. The turn-off process begins by applying the negative gate voltage at time t_0. By discharging the input capacitance of the IGBT, the gate-emitter voltage, v_{ge}, is decreased, but v_{ce} remains unchanged until v_{ge} falls completely where the IGBT condition is out of saturation. This period is denoted by t_{vd} in Fig. 4. After this time, the collector-emitter voltage increases. When v_{ce} reaches the forward blocking voltage, v_{ce0}, the free wheeling diode becomes forward-biased and begins to take over the load current. The collector current i_c drops rapidly. The fast decrease in the current through the parasitic inductance produces an overshoot in the voltage v_{ce} [9] - [10].

3.2.3 Diode turn-off loss

The turn-off switching behavior of the diode is shown in Fig. 5. The diode current, i_d, is assumed to be linearly declined in the time interval of t_0 and t_2. After t_2, the forward voltage drop begins to fall to $-v_d$. In the time duration between t_1 and t_2, the i_d is expressed as [9] :

$$i_d(t) = -I_1 \times (t - t_1) \times e^{-\alpha_1 (t - t_1)^2} \quad (2)$$

where

$$I_1 = \sqrt{2\alpha_1}\, I_{rr} e^{\frac{1}{2}},$$

$$\alpha_1 = \frac{1}{2(Kt_{rr})^2},$$

$$K = \frac{t_{rra}}{t_{rr}}$$

During the period $t > t_2$,

$$i_d(t) = I_{rr} e^{-\alpha_2 (t - t_2)^2} \quad (3)$$

Table 1 Device Parameters for inverters
$V_{CES} = 1200[V],\ T = 25^{\circ}$

Device / Parameter	Type A	Type B	Type C	Type D
$V_{CE0}(V)$	1	0.6	1.2	1.2
$V_{CE(Sat)}(V)$	2.5	1.3	2.8	3.2
$V_{GE}(V)$	15	15	15	15
$V_F(V)$	1.8	1.4	1.8	2.8
$V_{F0}(V)$	0.8	0.8	0.8	1.3
$E_{on}(mJ)$	4.1	3	1.2	3
$E_{off}(mJ)$	3.5	2.5	1.8	2.5
$E_{rr}(mJ)$	1	1.1	1	3
$t_{on}(\mu s)$	0.015	0.3	0.01	0.23
$t_{off}(\mu s)$	0.35	0.13	0.11	0.3

Type-A : Semikron SKM 100GB123D
Type-B : Infineon FF100R12RT4
Type-C : Fuji Electronic 2MBI100HB-120-50
Type-D : Microsemi APT50GT120LRDQ2(G)

Table 2 Device parameters for inverters
$V_{CES} = 600[V],\ T = 25^{\circ}$

Device / Parameter	Type A	Type B	Type C	Type D
$V_{CE0}(V)$	0.8	0.9	0.9	0.9
$V_{CE(Sat)}(V)$	1.6	1.8	1.8	2.4
$V_{GE}(V)$	15	15	15	15
$V_F(V)$	1.7	1.6	2	2.8
$V_{F0}(V)$	0.6	0.7	0.9	1.2
$E_{on}(mJ)$	1.8	1.45	0.6	1.8
$E_{off}(mJ)$	2.1	0.91	1.2	0.7
$E_{rr}(mJ)$	0.5	2	0.4	0.5
$t_{on}(\mu s)$	0.06	0.02	0.35	0.13
$t_{off}(\mu s)$	0.31	0.22	0.3	0.2

Type-A : Semikron SKM 75GAL063D
Type-B : Infineon IKW50N60H3
Type-C : Fuji Electronic 2MBI 100N-060
Type-D : Microsemi APT30GP60BDQ1(G)

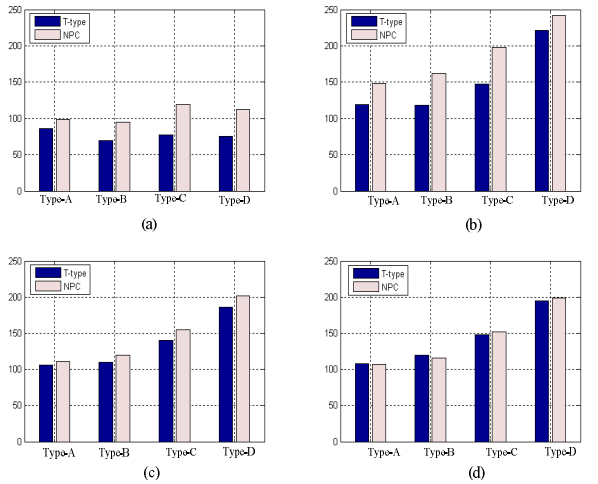

Fig. 6 Conduction loss of three-level T-type and NPC converters in different conditions (a) MI=1, PF=1, (b) MI=1, PF=-1, (c) MI=0.5, PF=0, (d) MI=0.1, PF=0.5

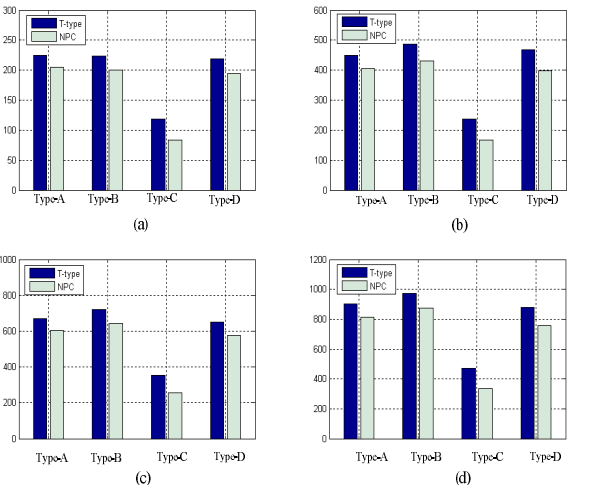

Fig. 7 Switching loss of three-level T-type and NPC converters in different switching frequencies (a) $F_s = 10[kHz]$, (b) $F_s = 20[kHz]$, (c) $F_s = 30[kHz]$, (d) $F_s = 40[kHz]$.

where α_2 is a constant which determines the rate at which the reverse recovery current decays less than 10% of I_{rr} at t_3 in Fig. 5 [10]-[12].

3.2.4 Calculation of switching losses

The switching losses can be estimated from the approximation of the switching characteristics of the IGBT and diode [7]-[9]. However, the more convenient way for calculating the switching losses is to utilize the switching energy-current (E-I) characteristic for on and off times. The IGBT switching losses can be calculated in (4) for the turn-on and turn-off energy in IGBTs and diodes [5]-[7].

$$P_{on+off} = \frac{1}{\pi} \cdot f_s \cdot [E_{on}(i) + E_{off}(i)] \tag{4}$$

where E_{on} is the on energy and E_{off} is the off energy, which are a function of the current. Also, these parameters vary according to the junction temperature [17]-[20].

4. Comparison of Power Losses

It is known that the topology, components, and operating parameters (voltage, current and switching frequency) of the inverters affect the power loss.

A 33-kW system for the three-phase three-level T-type and NPC inverters is designed for a loss evaluation, where the output voltage and frequency are 380 V and 60 Hz, respectively.

The DC-link voltage is 600 V, in which each capacitance of the two DC-link capacitors is chosen as 2500 μF. An RL load is applied to the inverter and the load current is about 50 A. In the T-type inverter, 1,200-V rating of IGBTs is used in the leg and 600-V rating of IGBTs is adopted in the crossbar.

Also, the four device models are selected for the power loss comparison. The selected modules are listed as Semikron (Type-A), Infineon (Type-B), Fuji Electronic (Type-C) and Microsemi (Type-D) Co. The rated current of each module is 100 A. The conduction and switching losses are calculated from the parameters listed in Table 1 and 2 [17]-[20].

Fig. 6 shows the conduction loss comparisons of T-type and NPC three-level inverters in the case of different PF and MI. Here, the T-type inverter has the lower conduction loss than NPC inverter in the different MI and PF. The switching loss results at the different switching frequencies are shown in Fig 7. It is obvious that by increasing the switching frequency, the switching loss is increased. The T-type inverter has slightly higher switching loss than the NPC inverter.

Fig. 8 shows the total power losses with regard to the switching frequency for the T-type and NPC inverters in the case of MI=1 and PF=1. It is shown that the power loss of the T-type inverter is lower than that of the NPC inverter in low and medium switching frequency ranges. The crossing point (CP) in Fig. 8 depends on the device model.

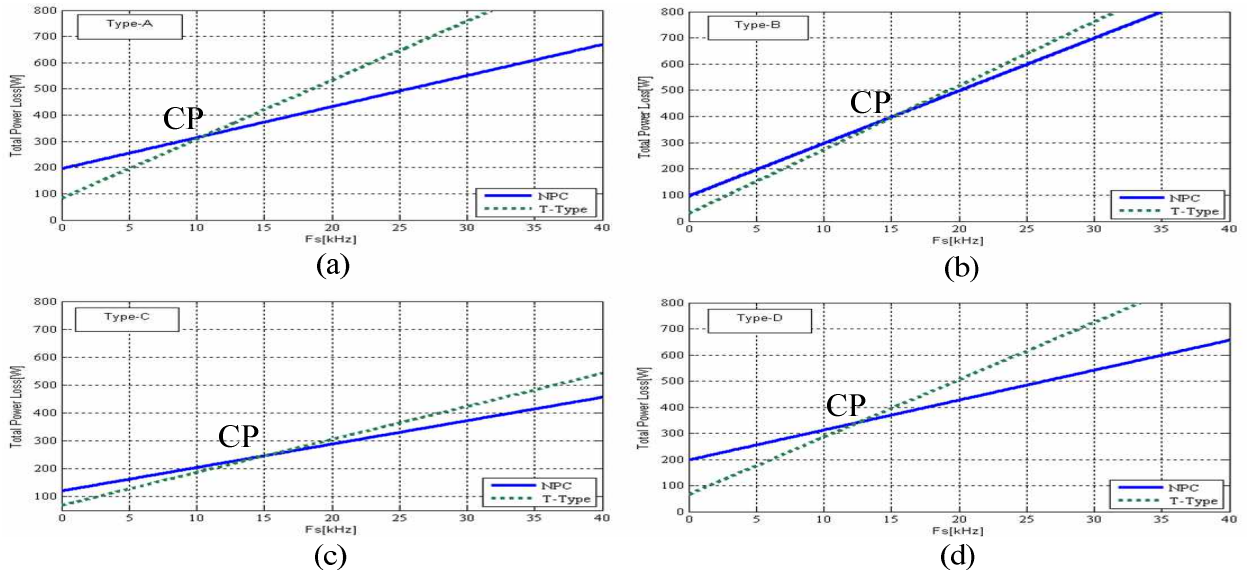

Fig. 8 Total power losses in different device models in MI=1, PF=1. (a)Type-A, (b) Type-B, (c) Type-C, (d) Type-D

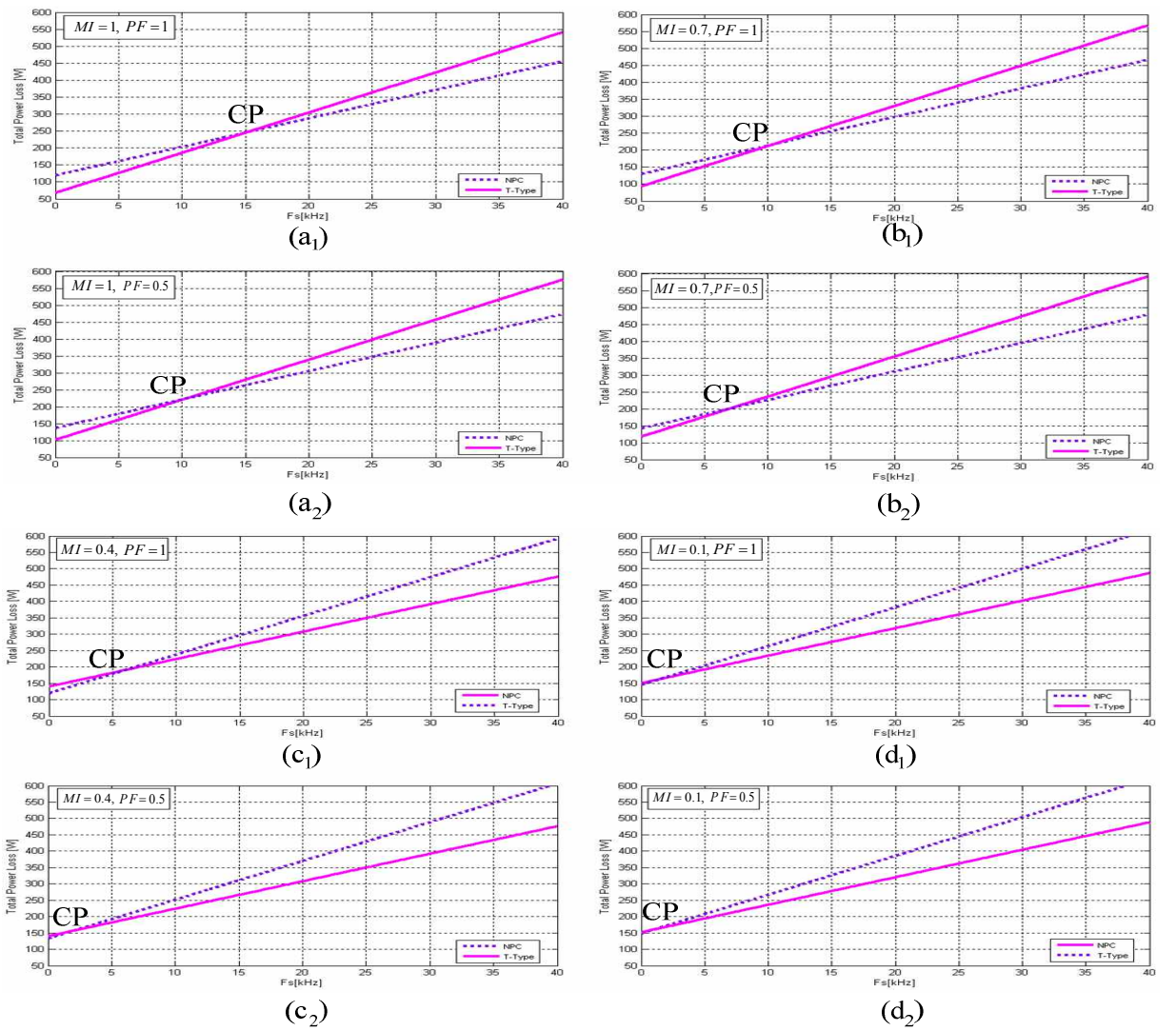

Fig. 9 Total power losses in type-C in different conditions

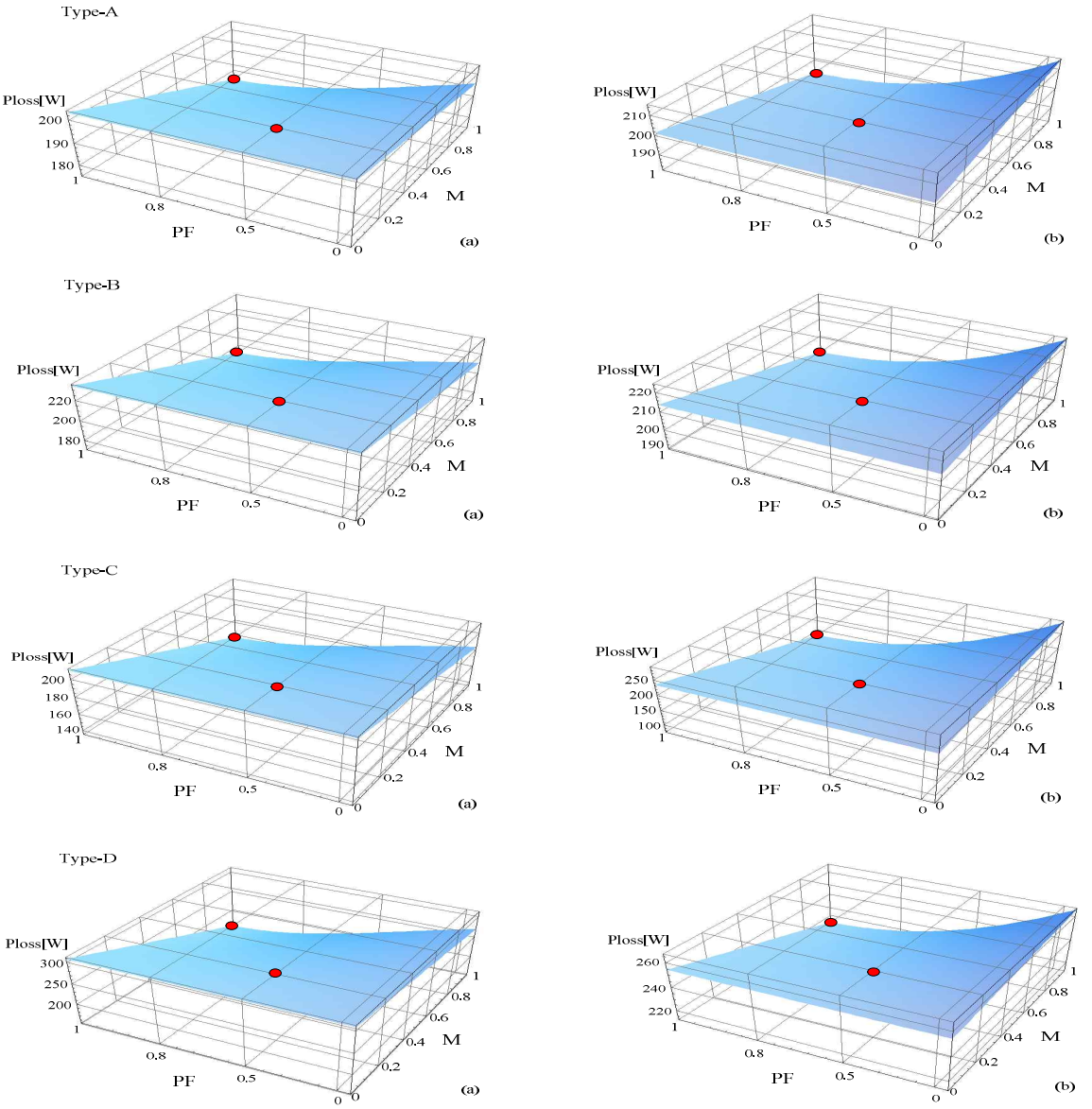

Fig. 10 The 3-D plot of total power loss as a function of MI and PF (a) T-type, (b) NPC-type

Table 3 Analysis and simulation results of total power loss in T-type and NPC-type for different devices

Total Power Loss [W] / Device		Operating Points			
		M = 1, PF = 1		M = 0.2, PF = 0.5	
		Analysis results	Simulation results	Analysis results	Simulation results
Type-A	T-Type	180.4	181	201	199.79
	NPC	240.7	222	202	200.06
Type-B	T-Type	163.7	175	213	221.31
	NPC	190.2	203	219	211.82
Type-C	T-Type	144.9	152	201	197.29
	NPC	171.6	201	203	204.34
Type-D	T-Type	177.0	178	244	288.18
	NPC	241.7	218	262	257.63

For instance, in the case of type-A, the CP is about 10 kHz. For the type-B and C, it is about 15 kHz. In the case of the type-D, the CP is slightly lower than 15 kHz. The NPC topology produces lower power loss in the switching frequency higher than the CP. To investigate the effect of the MI and PF on the total power losses, the type-C, for example, is selected.

Fig. 9(a1) shows the total power losses of type-C devices for the two inverters at MI=1 and PF=1. By changing the PF with the MI=1 kept, Fig. 9(a2) shows the crossing point moves to the lower switching frequency range which makes the NPC-type more efficient than the T-type in the medium switching frequency range. To show the effect of PF on total power loss, the analysis is done in the two PF cases of 0 and 0.5. For instance, in the case of MI=0.4 the power loss of the NPC inverter is lower than that of the T-type in the medium switching frequency range, which is shown in Fig. 9(c1). By changing the PF in Fig. 9(c2), the power losses of the NPC inverter is lower even in the low switching frequency range. Fig. 9(d1) and Fig.9(d2) show the power loss comparison in MI=0.1. It is obvious that the NPC inverter has the lower power losses compared with the T-type inverter in the whole range of switching frequency.

In Fig. 10, the 3-D plot of the total power losses versus MI and PF for the four devices is plotted. The switching frequency is selected as 5 kHz. To make the comparison clear, the two points are selected in the graphs to verify with the simulation results and Table 3 presents the selected point values in 3-D plot. It is evident that the T-type inverter mostly has lower power loss than the NPC type, which is reverse in the case of low MI.

5. Power Loss Evaluation by Simulation

The power loss analysis is verified by simulation. The inverter operates at the same conditions as analysis aforementioned. The DC-link voltage is 600 V and the load current is about 50 A. The forward voltage is added by data sheet parameters. The on-resistances of IGBTs and diodes are calculated by the parameters in data sheet and inserted in the simulation package of devices to model the conduction losses.

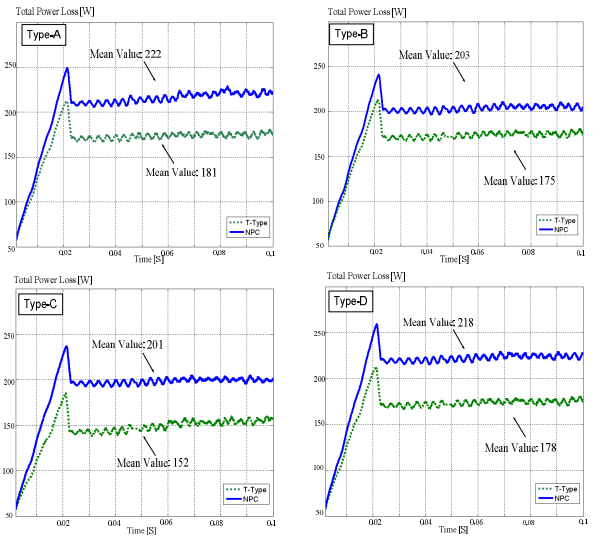

Fig. 11 Measured power loss in M=1 and PF=1

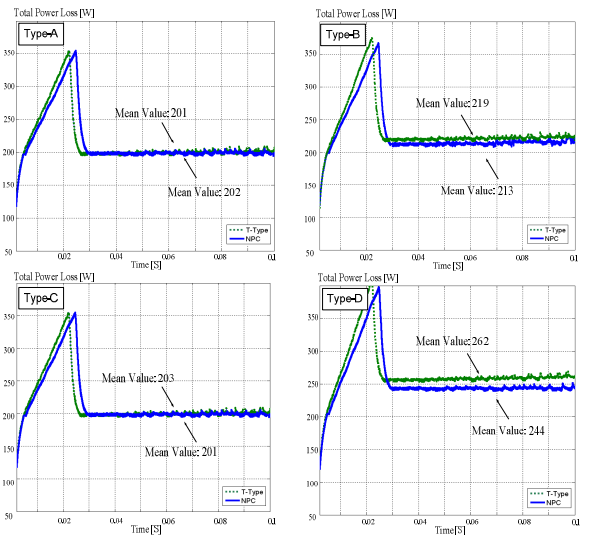

Fig. 12 Measured power loss in M=0.2 and PF=0.5

$$r_{oT} = \frac{V_{CE(Sat)} - V_{CE0}}{I_c}, \quad r_{oD} = \frac{V_F - V_{F0}}{I_c} \tag{5}$$

The switching loss is found by using the turn-on and off times of IGBTs and diodes from the parameters in Table 1 and 2.

The total power loss of the inverter is obtained from the difference between the measured input and output power. The simulation is carried out in the two conditions. In the first case, the MI is 1 and in the second case, the MI is 0.2 which is done in the two different power factors.

Fig. 11 shows the measured power loss in the T-type and NPC inverters in the case of MI=1 and PF=1. The total power losses for each type are illustrated, which are compared with analysis results. It is shown in the first and second columns of Table 3.

Fig. 12 illustrates the simulation results in the condition of MI=0.2 and PF=0.5. The data in the third and fourth columns of Table 3 show the results for analysis and simulation, respectively. A difference between the simulation results and the calculated values is insignificant, which is accepted.

6. Conclusions

In this paper, the evaluation of power loss for the three-level NPC and T-type inverters using the four different models of devices has been investigated. A loss analysis shows that in the case of maximum MI and unity PF, the T-type inverter is more efficient than the NPC type up to 10 kHz in type-A. The 'CP' is 15 kHz in type-B and -C and slightly lower than 15 kHz in type-D. However due to the effect of MI and PF on power losses, in the case of lower MI, the NPC inverter losses become lower than that of T-type in the medium frequency range. For instance in the case of MI equal 0.1, the 'CP' moves to the low switching frequency. Then, the power loss of the NPC-type becomes lower even in the low switching frequency range. Not only MI but also lower PF (0.5) affect the power loss. It is shown from analysis that the effect of MI is much higher than that of PF. The validity of the power loss analysis has been verified by simulation results. The results of device power loss calculated by the two methods coincide well with each other.

Acknowledgement

This research was supported by Basic Science Research Program through the National Research Foundation of Korea (NRF) funded by the Ministry of Education, Science and Technology (NRF-2012R1A1 A4A01015362).

References

[1] J. S. Lai and F. Z. Peng, "Multilevel converters. A new breed of power converters," *IEEE Trans. on Ind. Applicat.*, Vol. 32, No. 3, pp. 509-517, May/Jun. 1996.

[2] J. Rodriguez, J.-S. Lai, and F. Z. Peng, "Multilevel inverters: A survey of topologies, controls, and applications," *IEEE Trans. on Ind. Applicat.*, Vol. 49, No. 3, pp. 724-738, Aug. 2002.

[3] L. G. Franquelo, J. Rodriguez, J. I. Leon, S. Kouro, R. Portillo and M. A. M. Prats, "The age of multilevel converters arrives," *IEEE Industry Electronics Magazine*, pp. 28-39. June 2008.

[4] J. Rodriguez, L. G. Franquelo, S. Kouro, J. I. Leo´n, R. C. Portillo, M. A. M. Prats and M. A. Pe´rez, "Multilevel converters: an enabling technology for high-power applications," *Proc. of the IEEE*, Vol. 97, No. 11, pp. 1786-1817, Nov. 2009.

[5] M. Schweizer, and J. W. Kolar, "Design and implementation of a highly efficient three-level T-type converter for low-voltage applications," *IEEE Trans. on Power Electron.*, Vol. 28, No. 2, pp. 899-907, Feb. 2013.

[6] R. Teichmann and S. Bernet, "A comparison of Three level converters versus two level converters for low voltage drives, traction and utility applications," *IEEE Trans. on Ind. Applicat.*, Vol. 41, No. 3, pp. 855-865, May/Jun. 2005.

[7] T-J. Kim, D-W Kang, Y-H. Lee, and D. S. Hyun, "The analysis of conduction and switching losses in multi-level inverter system," *Proc in. IEEE PESC*, pp. 1363-1368, Jun. 2001.

[8] Semikron Application Note (AN-11001).

[9] P. K. Chaturvedi, S. Jain, P. Agrawal, R. K. Nema, and K. K. Sao, "Switching losses and harmonic investigation in multilevel inverters," *IETE Journal of Research*, Vol. 54, No. 4, pp. 297-307, Nov. 2009.

[10] D. Andler, S. Kouro, M. Perez, J. Rodriguez, and Bin Wu, "Switching loss analysis of modulation methods used in neutral point clamped converters," *Proc in. IEEE ECCE*, pp. 2565-2571, Sep. 2009.

[11] J. W. Kolar, H. Ertl and F. C. Zach, "Influence of the modulation method on the conduction and switching losses of a PWM inverter system," *IEEE Transa. on Ind. Applicat.*, Vol. 27, No. 6, pp. 1063-1075, Nov/Dec. 1999.

[12] G-I. Orfanoudakis, S. M. Sharkh, M. A. Yuratich, and M. A. Abusara, "Loss comparison of two and three-level inverter topologies," *Proc in. IET. PEMD*, pp. CD-ROM Format, April 2010.

[13] P. Alemi and D.-C. Lee, "Power loss comparison in two-and three-level PWM converters," *Proc in. ICPE*, pp. 1452-1457, May/Jun. 2011.

[14] U. Drofenik and J. W. Kolar, "A general scheme for calculating switching-and conduction-losses of power semiconductors in numerical circuit simulations of power electronic systems," *Proc. in. IPEC,* pp. CD-ROM Format, April 2005.

[15] A. D. Rajapakse, M. Gole, and P. L. Wilson, "Approximate loss formula for estimation of IGBT switching losses through EMTP-type simulations," *Proc in. Int. Conf of Power System. IPST*, pp. CD-ROM Format, Jun. 19-23, 2005.
[16] A. D. Rajapakse, M. Gole, and P. L. Wilson, "Electromagnetic transients simulation models for accurate representation of switching losses and thermal performance in power electronic systems," *IEEE Trans. on Power Delivery*, Vol. 20, No. 1, pp. 319-327, Jan. 2005.
[17] Eupec-Infineon IGBT/ Diode module data sheets. Online. Available: www.infineon.com/eupc.
[18] Microsemi IGBT/ Diode module data sheets. Online. Available: www.microsemi.com/
[19] Semikron IGBT/ Diode module data sheets. Online. Available: www.semikron.com.
[20] Fuji electric IGBT/ Diode module data sheets. Online. Available: www.fujielectric.com.

Appendix:

A.1 NPC Three-level Inverter

The conduction losses for the IGBTs and anti-parallel diodes in one leg of the NPC inverter are calculated by (6) - (10) in [8].

- S_{a1} and S_{a4}

$$P_{Cond} = \frac{MI}{12\pi}.3\,V_{CE0}.[(\pi-\varphi).\cos(\varphi)+ \\ +\sin(\varphi)]+2r_{ce}I.(1+\cos(\varphi))^2 \quad (6)$$

- S_{a2} and S_{a3}

$$P_{Cond} = \frac{I}{12\pi}.V_{CE0}.[12+3M(\varphi.\cos(\varphi))-\sin(\varphi))]+ \\ r_{ce}.I.(3\pi-2M(1-\cos(\varphi))^2) \quad (7)$$

- D_5 and D_6

$$P_{Cond} = \frac{I}{12\pi}.V_{F0}.[12+3M(2\varphi-\pi).\cos(\varphi) \\ -2\sin(\varphi))]+r_f.I.(3\pi-4M(1+\cos(\varphi))^2) \quad (8)$$

- D_1 and D_4

$$P_{Cond} = \frac{MI}{12\pi}.3\,V_{F0}.[(-\varphi).\cos(\varphi)+ \\ +\sin(\varphi)]+2r_fI.(1-\cos(\varphi))^2 \quad (9)$$

- D_2 and D_3

$$P_{Cond} = \frac{I}{12\pi}.V_{F0}.[12+3M(\varphi.\cos(\varphi))-\sin(\varphi))]+ \\ r_f.I.(3\pi-2M(1-\cos(\varphi))^2) \quad (10)$$

A.2 T-Type Three-level Inverter

The conduction losses for the IGBTs and anti-parallel diodes in one leg of the T-type inverter are calculated by (11) - (14) in [8].

- S_{a1} and S_{a4}

$$P_{Cond} = \frac{MI}{12\pi}.3\,V_{CE0}.[(\pi-\varphi).\cos(\varphi)+ \\ +\sin(\varphi)]+2r_{ce}I.(1+\cos(\varphi))^2 \quad (11)$$

- S_{a2} and S_{a3}

$$P_{Cond} = \frac{I}{12\pi}.V_{CE0}.[12+6M(\varphi.\cos(\varphi))-\sin(\varphi)) \\ -3M\pi\cos(\varphi)]+r_{ce}.I.(3\pi-4M(1+\cos(\varphi))^2) \quad (12)$$

- D_2 and D_3

$$P_{Cond} = \frac{I}{12\pi}.V_{F0}.[12+3M(2\varphi.\cos(\varphi))-2\sin(\varphi)) \\ -3M\pi\cos(\varphi)]+r_f.I.(3\pi-4M(1+\cos(\varphi))^2) \quad (13)$$

- D_1 and D_4

$$P_{Cond} = \frac{MI}{12\pi}.3\,V_{F0}.[(-\varphi).\cos(\varphi)+ \\ +\sin(\varphi)]+2r_fI.(1-\cos(\varphi))^2 \quad (14)$$

where,

$$r_{ce} = \frac{V_{CE}-V_{CE0}}{I},\quad r_f = \frac{V_F-V_{F0}}{I}$$

and:

I: rated current.
V_{CE} : rated collector-emitter voltage.
V_{CE0} : threshold voltage of IGBT.
V_F : diode voltage drop at rated current
V_{F0} : threshold voltage of diode (0.7V)
M : modulation index$(0 \le M \le 1)$
φ : power factor angle
r_{ce} : IGBT forward resistance
r_f : Diode forward resistance

Payam Alemi was born in Tabriz, Iran in 1982. He received the B.Sc. degree from the University of Tabriz, Tabriz, Iran in 2005 and the Msc. degree from the science and research branch Tehran Azad university in 2008. He is currently working toward his Ph.D degree. His research interests include the control of multilevel power converters and power loss analysis for converters and machine drives.

Dong-Choon Lee received his B.S., M.S., and Ph.D. in Electrical Engineering from Seoul National University, Seoul, Korea, in 1985, 1987, and 1993, respectively. He was a Research Engineer with Daewoo Heavy Industry from 1987 to 1988. Since 1994, he has been a Professor in the Department of Electrical Engineering, Yeungnam University, Gyeongbuk, Korea. As a Visiting Scholar, he joined the Power Quality Laboratory, Texas A&M University, College Station in 1998, and the Electrical Drive Center, University of Nottingham, U.K. in 2001, and the Wisconsin Electric Machines and Power Electronic Consortium, University of Wisconsin, Madison in 2004, and the FREEDM Systems Center, North Carolina State University, Raleigh, U.S.A. from September, 2011 to August 2012. Currently, he is a Publication Editor of Journal of Power Electronics. His research interests include AC machine drives, control of power converters, renewable energy system, and power quality.